Wireless Micromachined Ceramic Pressure Sensor for High-Temperature Applications

Michael A. Fonseca, *Member, IEEE*, Jennifer M. English, Martin von Arx, and Mark G. Allen, *Member, IEEE*

***Abstract*—In high-temperature applications, such as pressure sensing in turbine engines and compressors, high-temperature materials and data retrieval methods are required. The microelectronics packaging infrastructure provides high-temperature ceramic materials, fabrication tools, and well-developed processing techniques that have the potential for applicability in high-temperature sensing. Based on this infrastructure, a completely passive ceramic pressure sensor that uses a wireless telemetry scheme has been developed. The passive nature of the telemetry removes the need for electronics, power supplies, or contacts to withstand the high-temperature environment. The sensor contains a passive *LC* resonator comprised of a movable diaphragm capacitor and a fixed inductor, thereby causing the sensor resonant frequency to be pressure-dependent. Data is retrieved with an external loop antenna. The sensor has been fabricated and characterized and was compared with an electromechanical model. It was operated up to $400\ ^{\circ}\mathrm{C}$ in a pressure range from 0 to 7 Bar. The average sensitivity and accuracy of three typical sensors are: $-141\ \mathrm{kHz\,Bar^{-1}}$ and 24 mbar, respectively. [662]**

***Index Terms*—Capacitive sensor, ceramic, high temperature, low-temperature cofireable ceramic (LTCC), pressure sensor, screen-printed.**

I. Introduction

In high-temperature applications, such as pressure sensing in turbine engines and compressors, high-temperature materials are required. Pressure sensors inside a turbine engine, for example, monitor surface pressure differentials and temperature gradients [1], [2]. In an aircraft engine, the measurement of the air-pressure as it reaches the combustor helps to control the air/fuel mixture to reduce the risk of stall. This requires a sensor that operates in a turbulent gas environment at elevated temperatures from 600 to 1800 °C and provides an incentive for the development of high-temperature pressure sensors.

Micromachined pressure sensors are an established commercial product [32]. A typical pressure sensor is based on a flexible silicon membrane as the sensing element and uses silicon piezoresistors or capacitors for data retrieval. These sensors have been documented extensively [4]. However, these devices have typically not been used in extremely high-temperature environments for both materials and readout reasons.

Manuscript received February 7, 2001; revised January 22, 2002. This work was supported in part by the Army Research Office under the Intelligent Turbine Engines MURI Program, Contract DAAH049610008, under the supervision of Dr. D. Mann. Subject Editor G. B. Hocker.

The authors are with the School of Electrical and Computer Engineering, Georgia Institute of Technology, Atlanta, GA 30332-0269 USA (e-mail: gt8456b@prism.gatech.edu).

Publisher Item Identifier 10.1109/JMEMS.2002.800939.

Potential high-temperature materials have been investigated as an alternative to silicon. Silicon carbide, polycrystalline diamond and ceramic materials have been reported as high-temperature materials for sensor fabrication [5], [6]. Silicon carbide pressure sensors employ the flexible membrane design and use piezoresistors to measure pressure changes. The incorporation of silicon carbide circuitry is also possible in order to retrieve the pressure data. Polycrystalline diamond pressure sensors also employ a flexible membrane and piezoresistors. These technologies show great promise for integrated high-temperature pressure sensors, but their manufacturing infrastructure is not nearly as well developed as that for silicon and electronic packages for silicon.

The microelectronics packaging industry offers a well-developed ceramic packaging procedure using ceramic cofireable tape. The ceramic tape consists of alumina particles and glass particles suspended in an organic binder, which is subsequently fired to form a ceramic structure. In general, this type of tape is referred to as low-temperature cofireable ceramic (LTCC) as the typical curing (firing) temperature is $900\ ^{\circ}\mathrm{C}$ [7]. Ceramic tapes made solely from alumina particles are also available and have curing temperatures above $1600\ ^{\circ}\mathrm{C}$. These high-temperature characteristics indicate that the ceramic tape may be an excellent choice for the fabrication of pressure sensors for high temperatures.

In this work, a pressure sensor for high-temperature applications based on LTCC fabrication technology is realized. A passive wireless resonant telemetry scheme, which is well known in sensor technology [8]–[10], is employed to measure the pressure. In this scheme, the pressure is translated into a frequency shift output, which can be detected remotely. This scheme is ideally suited for high-temperature sensing, since the passive nature of the telemetry removes the need for electronics, power supplies, or contacts to withstand the high-temperature environment, thereby allowing the sensor to operate at temperatures that are ideally limited only by materials.

II. Design and Fabrication

A schematic of the wireless pressure sensor is shown in Fig. 1(a) [8]. The sensor consists of two diaphragms, separated by a vacuum-sealed cavity of gap size t_g. The stack of diaphragms and cavity is enclosed by two electrodes that form a capacitor. If a pressure P is applied the gap size of the cavity between the two membranes is reduced and the capacitor value increases. The capacitor is electrically connected to a planar spiral inductor coil. These components form a passive

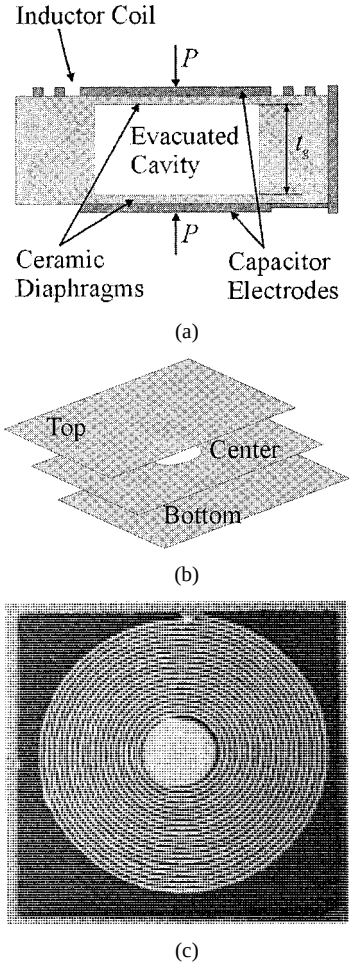

Fig. 1. (a) Schematic cross section, (b) layered construction, and (c) top-view photograph of a ceramic pressure sensor with silver screen printed conductors.

LC resonator with resonant frequency f_o, which is pressure dependent. To achieve passive wireless telemetry, the sensor is placed inside an external loop antenna coil and the impedance and phase response of the antenna coil are measured as a function of frequency.

The sensors are fabricated using multiple sheets of Dupont 951AT ceramic tape [7]. The tape consists of alumina and glass particles suspended in an organic binder. The structure of the sensor is comprised of three sections illustrated in Fig. 1(b). Each section consists of two sheets of ceramic green tape, which has been cut into square shapes with an area of approximately 16cm^2 and a thickness of approximately $100\,\mu$m. The top and bottom sections create the pressure sensitive membranes of the mechanical structure. The center section contains a circular hole of radius a to form the evacuated cavity.

To form the sensor, the ceramic sheets are laminated together in a hot vacuum press for 5 min, rotated horizontally 180° and pressed for 5 min again. The press temperature used is 70 °C with a pressure of 3000 psi (9.38 tons for an area of 6.25in^2). After lamination, the sample is cut down to a square approximately 3.8 cm on a side prior to firing. The sample is fired in a box furnace in air for 30 min at 500 °C (5 °C min^{-1} ramp rate) to bake off the organics and then for 20 min at 850 °C (5°C min^{-1} ramp rate) to melt the glass particles and harden the sample [7].

The inductor coils and capacitor electrodes of the pressure sensor were fabricated using screen-printing. Dupont 6160 silver ink, which is shrinkage-matched to the ceramic material, was used as a conductor material. The ink was dried in an oven at 120 °C for 10 min and then fired along with the firing of the green tape as described above.

III. Modeling

The electromechanical model of the ceramic pressure sensor is derived in three steps. First, the load-deflection part gives the center deflection d_o of the membranes as a function of applied pressure P. Next, the pressure dependent capacitor $C_s(P)$ is calculated as a function of d_o. This capacitance determines the resonant frequency of the sensor. Finally, the coupled system antenna and sensor is analyzed.

The sensor model is illustrated in Fig. 2(a). The deflection of the diaphragms is calculated using thin plate theory, in which the effects of both bending and stretching of the diaphragm are considered. Several assumptions are made:

i) the edges of the diaphragm are clamped and can be modeled by built-in boundary conditions;
ii) no residual stress is present in the diaphragms since the diaphragms as well as the rest of the sensor are fabricated from the same material;
iii) the diaphragms are subject to a uniform load P.

Using these assumptions and large deflection theory for circular plates a model of the diaphragm shape is given by

$$d = d_o\left(1 - \frac{r^2}{a^2}\right)^2 \tag{1}$$

where d_o is the center deflection and is given by the equation

$$\frac{d_o}{t_m} + 0.488\left(\frac{d_o}{t_m}\right)^3 = \frac{3P(1-\nu^2)}{16E}\left(\frac{a}{t_m}\right)^4 \tag{2}$$

where a is the plate radius, E is Young's Modulus and ν is Poisson's ratio of the plate [12].

The maximum strain allowed before either plastic deformation or plate rupture occurs is determined by [12]

$$\varepsilon_{\max} = \frac{32d_o^2}{27a^2} \tag{3}$$

which, when given the material property of ultimate strain, allows the maximum size of the gap t_g of the cavity to be determined. Using (2) and (3), as well as constraints imposed by fabrication, the optimum geometrical parameters (i.e., t_m, t_g, and a) for a given pressure range and desired maximum deflection can be calculated.

For example, consider a typical pressure sensor with the following design parameters: $a = 4.2$ mm, $t_m = 0.1$ mm. The Young's modulus E of the ceramic tape (as given by the manufacturer) is 152 GPa and the Poisson's ratio ν was assumed to be 0.3. The maximum deflection allowed before the diaphragm will rupture was determined from (3) using the rupture strain. The maximum strain $\varepsilon_{\max}$ of the Dupont 951-AT ceramic tape provided by the manufacturer is 0.0021, at room temperature. This maximum strain corresponds to a maximum deflection of 0.176 mm and a maximum pressure of 12.5 bar. As a result, a pressure

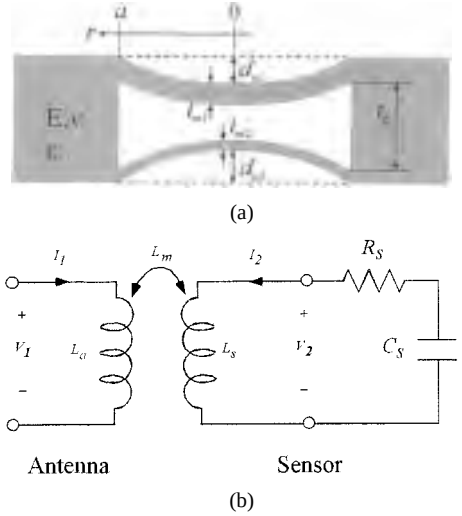

Fig. 2. (a) Schematic cross section of ceramic sealed cavity structure for mechanical modeling. (b) Equivalent circuit of electrical model for a sensor coupled with an antenna.

range from 0 to 12.5 bar is the predicted operating range for a diaphragm with the geometrical properties described.

The capacitor C_s for the pressure sensor consists of the top and bottom metal electrodes separated by the ceramic diaphragms and the cavity, as shown in Fig. 2(a). The capacitance at zero pressure is given by

$$C_o = \frac{\varepsilon_o \pi a^2}{t_g + 2t_m \varepsilon_r^{-1}}, \tag{4}$$

where a is the diaphragm radius, t_m and ε_r are the thickness and relative dielectric constant, respectively, of the ceramic diaphragms. A pressure dependent capacitor model is given by [13]

$$C_s(P) = C_o \sum_{i=0}^{\infty} \frac{1}{2i+1} \left(\frac{2d_o}{t_g + 2t_m \varepsilon_r^{-1}} \right)^i. \tag{5}$$

The sensor resonance and its coupling to the antenna is modeled with a two-port network using transformer theory, as shown in Fig. 2(b) [14]. The input impedance of the antenna is expressed with the electrical parameters of the sensor it encloses. Transformer network theory and Kirchhoff's law, using phasor notation ($s = j\omega = j2\pi f$), yields

$$V_1 = sL_a I_1 + sL_m I_2 \tag{6}$$

$$V_2 = sL_m I_1 + sL_s I_2 \tag{7}$$

and

$$-R_s I_2 - V_2 - \frac{1}{sC_s} I_2 = 0 \tag{8}$$

where L_a is the antenna inductance, L_s is the sensor inductance, L_m is the mutual inductance, C_s is the sensor capacitance, R_s is the sensor series resistance, and V_1, V_2, I_1 and I_2 are the transformer voltages and currents, respectively, in Fig. 2(b). Replacing V_2 in (8) with (7) and solving for I_2 yields

$$I_2 = I_1 \frac{-sL_m}{R_s + sL_s + \frac{1}{sC_s}}. \tag{9}$$

Substitution of I_2 in (6) and using (9) gives the antenna voltage V_1

$$V_1 = (sL_a) I_1 + \left(\frac{-s^3 L_m^2 C_s}{1 + L_s C_s s^2 + s R_s C_s} \right) I_1. \tag{10}$$

Substituting L_m with the coupling coefficient $k = L_m (L_a L_s)^{-1/2}$,

$$f_o = \frac{1}{2\pi} \left(\frac{1}{\sqrt{L_s C_s}} \right) \tag{11}$$

and $Q = 2\pi f_o L_s / R_s$ the input impedance is given by

$$Z_1 = \frac{V_1}{I_1} = j2\pi f L_a \left[1 + k^2 \frac{\left(\frac{f}{f_o}\right)^2}{1 - \left(\frac{f}{f_o}\right)^2 + \frac{1}{Q} j \frac{f}{f_o}} \right]. \tag{12}$$

This result relates the resonance frequency f_o of the sensor to the measurable quantity Z_1. By measuring Z_1 as a function of f, f_o can be extracted.

IV. Results

Measurements for the pressure sensors were taken using a Parr pressure/temperature vessel. The pressure can be controlled from atmospheric pressure up to 194 bar using a nitrogen gas tank, a Fisherbrand regulator and an Ashcroft pressure gauge. The temperature can be controlled from room temperature up to 800°C using a Waslow 4780 temperature controller and a thermocouple placed in proximity with the sensor. For the described measurements, the temperature ramp rate was 5 °C min^{-1} and a dwell time of 10 min was used. Sensors left at 400 °C over a 24-h period did not exhibit a change in resonance frequency or pressure sensitivity nor did they exhibit hysteresis.

Since the vessel is made of metal, the antenna must be placed inside the chamber for all the measurements. In the cases where there is no metal between the sensor and the antenna, the antenna can be placed outside of the harsh environment. However, even in the case where the antenna must be exposed to the harsh environment, the wireless scheme is advantageous since it eliminates the need for potentially unreliable, high-temperature contacts to be made with the sensor, and also allows for the possibility of the sensor to be mounted on moving parts. The antenna has an inductance of roughly 670 nH. The frequency dependent antenna impedance is measured using an HP9141A impedance analyzer. Feed-throughs in the vessel shell provide the connections between antenna and impedance analyzer. They have a parasitic cross-coupling capacitance of 0.202 pF. The self-resonance frequency of this system is 43 MHz, which is high enough for our purposes to avoid interaction with the sensor resonance.

The sensor was placed in the plane of the antenna loop and the impedance Z of the antenna was measured as a function of frequency. Fig. 3 shows the measured phase and magnitude of Z for sensor 1 at atmospheric pressure. Below and above resonance the phase is close to the ideal value of 90° for an inductor and the magnitude depends linearly on the frequency. At resonance, the sensor induces a change in impedance phase and magnitude. The phase minimum $f_{\min}$ occurs at 17.14 MHz.

The phase data were fit with (12), using Mathematica 4.0. The fit is shown as a solid line in Fig. 3(a). The resonance frequency f_o, the coupling coefficient k, and the quality factor Q obtained from the fit are 16.99 MHz, 0.190, and 61.9, respectively. Note

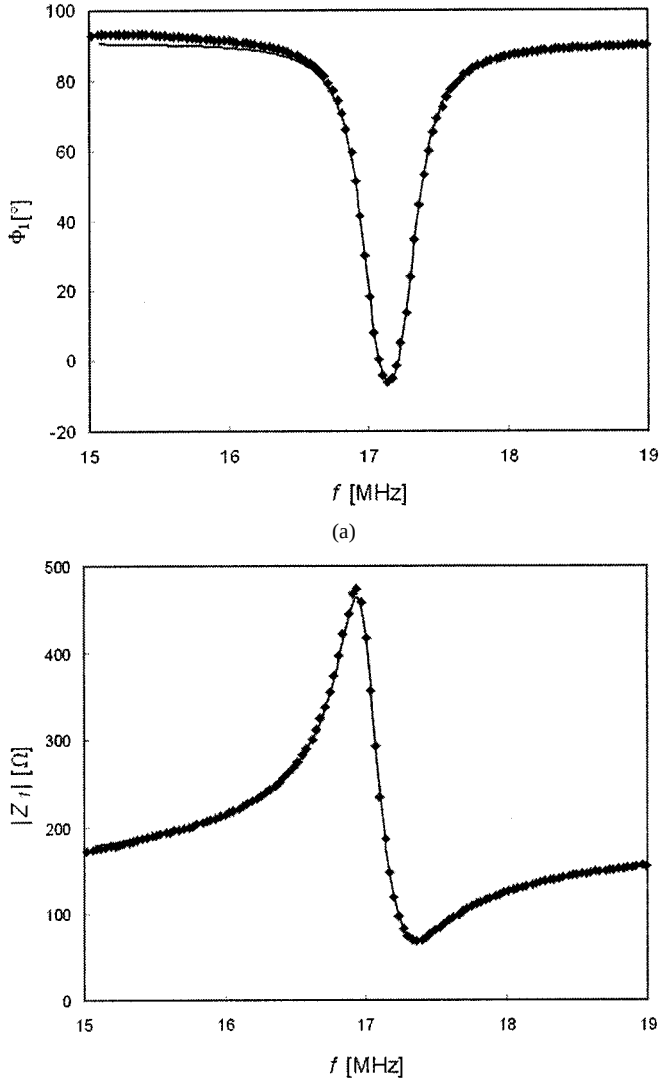

Fig. 3. Phase Φ_1 (a) and magnitude (b) of impedance Z_1 versus frequency. The measured data are shown as points while the optimum fit using (12) is shown as solid line.

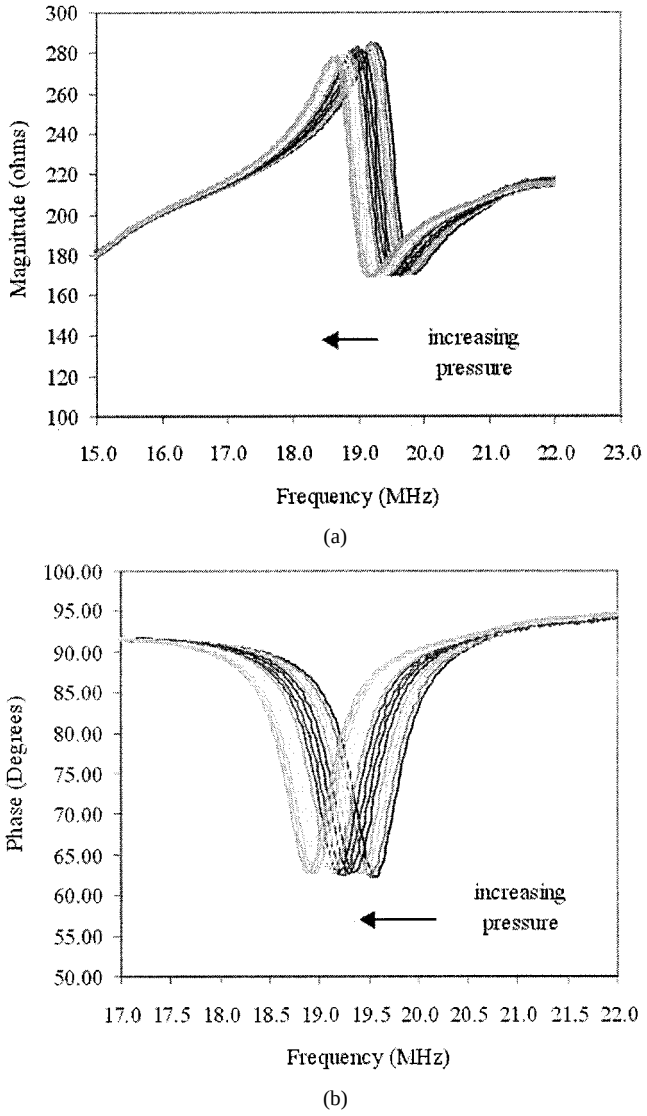

Fig. 4. Antenna coil magnitude (a) and phase (b) for a ceramic pressure sensor at room temperature for 0–7 bar pressure range.

that the phase minimum $f_{\min}$ is 0.92% higher than f_o. The difference is discussed by calculating the frequency, where phase minimum of Z_1 occurs from (12). The Taylor expansion of $f_{\min}$ in k and Q^{-1} is

$$f_{\min} = f_o\left(1 + \frac{k^2}{4} + \frac{1}{8Q^2}\right). \tag{13}$$

The difference between $f_{\min}$ and f_o can therefore be explained as an effect of the large coupling factor k in this measurement.

To fit the magnitude data in Fig. 3(b), the parameters f_o, k, and Q were kept the same as for the phase fit and the parameter L_a was optimized. The solid line in Fig. 3(b) shows fit data obtained with an optimal value of 1.67 μH for L_a.

Three sensors were characterized. Their resonance frequencies at zero pressure are 19.49 MHz, 16.99 MHz, and 22.68 MHz, respectively. Theoretical resonance frequencies at zero pressure were calculated using (4) and (11), yielding

$$f_o(P=0) = \frac{1}{2\pi}\sqrt{\frac{t_g + 2t_m\varepsilon_r^{-1}}{L_s\varepsilon_o\pi a^2}} = 43.76\ \text{MHz} \tag{14}$$

based on a capacitor electrode radius a and gap size t_g of 4.76 mm and 200 μm, respectively, and a diaphragm thickness t_m and relative dielectric constant ε_r of 200 μm and 7.8, respectively. The calculated and measured inductance L_s of the screen-printed coil are 6.7 and 4.2 μH, respectively. The theoretical resonance frequency is 93%–158% higher than the experimental results. The discrepancy between measured and predicted resonance frequencies was attributed to two effects. First, the capacitor electrodes are larger than the cavity, as indicated in Fig. 1(a). Second, the assumption of parallel field lines in the capacitor may not be valid at the boundary. Both effects increase the capacitance significantly because of the larger dielectric constant of ceramic compared to vacuum.

The magnitude and phase of Sensor 1 as a function of frequency and as parameterized by the applied pressure is shown in Fig. 4. The pressure dependence of the sensor can be obtained by determining the frequency at which the phase minimum of each curve occurs and plotting this frequency as a function of pressure. The pressure dependence of three nominally identical sensors as determined in this manner is shown in Fig. 5. Since

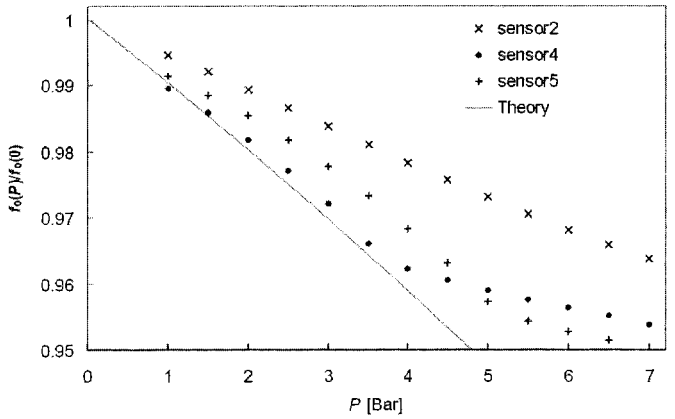

Fig. 5. Normalized resonance frequency f_o of three samples versus pressure P. The solid line denotes the theoretical pressure dependence according to model (15).

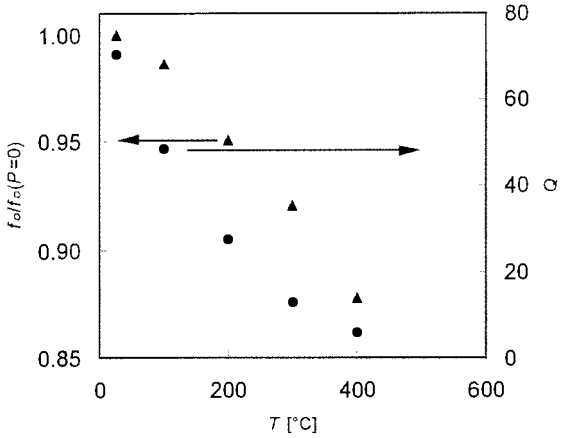

Fig. 6. Normalized resonant frequency f_o and quality factor Q versus temperature for sensor 1.

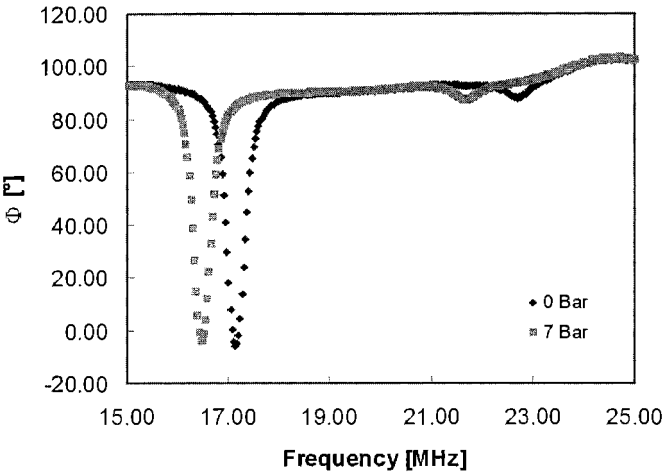

Fig. 7. Simultaneous readout of two sensors with different resonant frequencies. The phase Φ_1 of Z_1 is shown as a function of frequency at 0 bar and 7 bar.

no sensor data were taken at ambient vacuum (i.e., ambient pressure of zero bar), the first data points are at 1 bar. In order to compare with the theoretical development, which assumes a minimum differential pressure (as well as absolute pressure, since the reference pressure sealed in the cavity is ideally zero bar), the experimental data were extrapolated to a pressure of zero bar (yielding a zero pressure resonance frequency $f_o(0)$), and this extrapolated frequency was used to normalize the data points in accordance with the theory. At low pressures, f_o depends linearly on P. The sensitivities of the three samples are -105 kHz bar^{-1}, -154 kHz bar^{-1}, and -164 kHz bar^{-1} respectively, between 0 bar and 3 bar. Above 3 bar the sensitivities of sensors 4 and 5 are reduced. Sensor-to-sensor discrepancies may be influenced by the relatively nonreproducible initial curvature of the membranes, which is introduced during the vacuum lamination process and set during the firing process. This initial curvature was not included in the models discussed above. Based on an accuracy of 3.2 kHz of the measurement of f_o, the accuracy of the pressure sensing is calculated. The three samples have a pressure sensing accuracy of 31 mbar, 21 mbar, and 19 mbar, respectively, at room temperature.

The theoretical pressure dependence for f_o was calculated using (5) and (11), yielding

$$f_o(P) = f_o(P=0)\left(\sum_{i=0}^{\infty}\frac{1}{2i+1}\left(\frac{2d_o}{t_g+2t_m\varepsilon_r^{-1}}\right)^i\right)^{-(1/2)}. \tag{15}$$

These theoretical data are shown as a solid line in Fig. 5. A linearized sensitivity of -205 kHz/bar over the range 0–4 bar is obtained, in reasonable agreement with the measured data.

To determine the parasitic temperature sensitivity, the resonance frequency was measured as a function of temperature. Fig. 6 shows normalized resonance frequencies f_o between 25 °C and 400 °C for sensor 1. The average slope is -5.56 kHz °C^{-1} between 25 °C and 400 °C. This parasitic temperature dependence needs to be compensated if the sensor is exposed to temperature variations of more than -0.576°C. A possible compensation scheme utilizes integration of a second sensor with no pressure dependence on the same substrate, i.e., a sensor without cavity.

Fig. 6 also shows the quality factor Q of sensor 1 as a function of temperature. Q is reduced from 70.2 at 25 °C to 6.0 at 400 °C. The temperature dependence of the quality factor is attributed to the increase in resistivity with temperature of the inductor metal. This limits the range of operation to 300 °C. A higher temperature range can be achieved by optimization of the coil geometry.

The read-out scheme enables the measurement of multiple sensors in parallel. Fig. 7 shows phase data for an array of two sensors. Data for sensors 4 and 5 in Fig. 5 were obtained from this data. This confirms, that an array of sensors can be measured in parallel.

The use of ceramic as membrane material also allows to measurement at elevated pressures. Fig. 8 shows the pressure dependence of a device tested up to 100 Bar.

V. Conclusion and Outlook

The design, modeling, fabrication and testing of a wireless ceramic sensor are presented. The sensor is made from ceramic cofired tape to create a sealed cavity structure with a flexible ceramic membrane. The ceramic structure is integrated with a

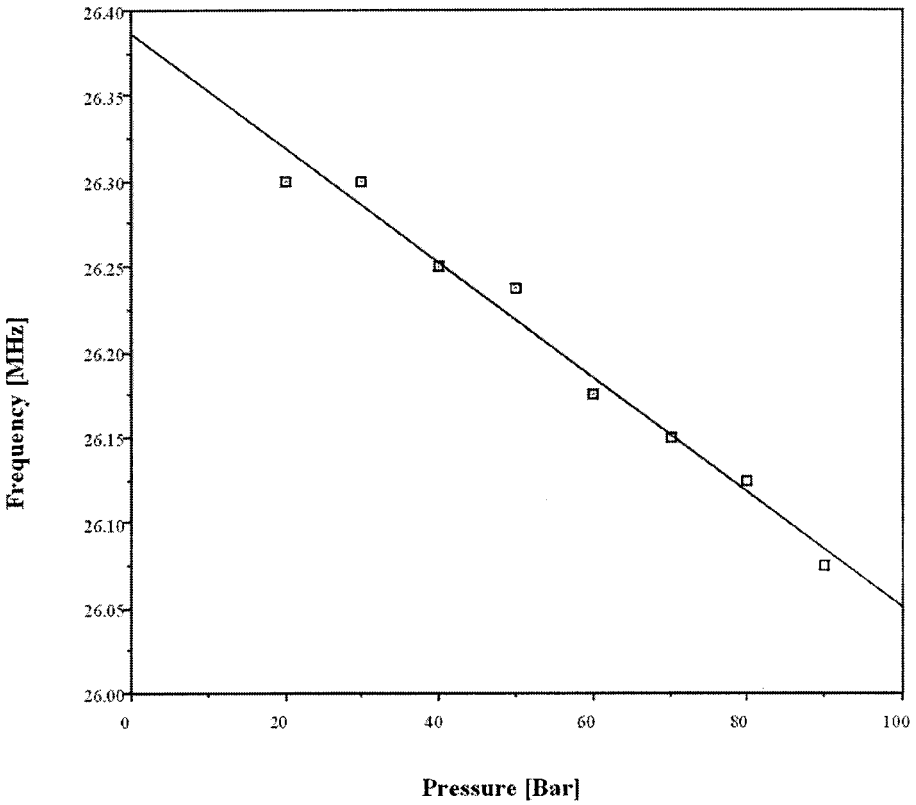

Fig. 8. High-pressure sensor data. The resonance frequency f_o is shown as a function of P.

varying C and fixed L resonant circuit. The resonant frequency of the sensor shifts with applied pressure. A passive wireless scheme is used to retrieve the pressure data.

An array of sensors with different resonance frequencies was characterized and successfully used to measure pressure up to 7 Bar. The average sensitivity and accuracy of three sensors are -141 kHz Bar^{-1} and 24 mbar. Its temperature dependence is -5.56 kHz °C^{-1} and will be compensated using a reference sensor co-integrated on the same substrate. The temperature range is currently limited to 400°C due to a reduction of the resonator quality factor with temperature.

Future optimization of the coil geometry and material will extend the range of operation to higher temperatures. The sensor structure will be redesigned to encapsulate the metal electrodes of the capacitor. Using a multi-layered coil will reduce the overall size of the sensor.

ACKNOWLEDGMENT

The authors would like to thank Professor D. Hertling and Professor R. Feeney of the Georgia Institute of Technology, Atlanta, for valuable technical discussion. Microfabrication was carried out in the Georgia Tech Microelectronics Research Center.

REFERENCES

[1] G. Smith, "The application of microtechnology to sensors for the automotive industry," *Microelectron. J.*, vol. 28, no. 4, pp. 371–9, May 1997.
[2] S. J. Prosser, "Advances in sensors for aerospace applications," *Sens. Actuators*, vol. A37–A38, pp. 128–34, 1993.
[3] W. P. Eaton and J. H. Smith, "Micromachined pressure sensors: Review and recent developments," *Proc. SPIE—The International Society for Optical Engineering*, vol. 3046, pp. 30–41, 1997.
[4] G. Blasquez, P. Pons, and A. Boukabache, "Capabilities and limits of silicon pressure sensors," *Sens. Actuators*, vol. 17, pp. 387–403, 1989.
[5] R. Okojie, A. Ned, D. Kurtz, and W. Carr, "6H-SiC pressure sensors for high temperature applications," in *Proc. 1996 IEEE/ASME MEMS Workshop*, 1996, pp. 146–149.
[6] E. Obermeier, "High temperature microsensors based on polycrystalline diamond thin films," in *Proc. 8th International Conference on Solid State Sensors and Actuators (Transducers '95)*, vol. 2, 1995, pp. 178–181.
[7] *Green Tape Material System, Design and Layout Guidelines*, Dupont Applied Technologies Group, pp. 1–17.
[8] D. L. Field, "Apparatus for Indicating an Abnormal Condition in a Vehicle Wheel," U.S. Patent 3 092 806, 1963.
[9] P. M. Wingfield, "Tuned Circuit Monitor for Structural Materials," U.S. Patent 3 906 340, 1975.
[10] Dezettel, "The grid-dip meter," *Electronics World*, pp. 50–51, Dec. 1960.
[11] J. English and M. G. Allen, "Wireless micromachined ceramic pressure sensors," in *Proc. Twelfth IEEE Microelectromechanical Systems Conf.*, 1999, pp. 511–516.
[12] S. P. Timeshenko, *Theory of Plates and Shells*. London, U.K.: McGraw Hill, 1984.
[13] S. P. Chang *et al.*, "A robust 8×8 capacitive pressure sensor array," in American Society of Mechanical Engineering Winter Annual Meeting, 1998.
[14] K. L. Su, *Fundamentals of Circuits, Electronics, and Signal Analysis*. New York: Houghton Mifflin Company, 1978, pp. 587–614.

Michael A. Fonseca (M'01) was born in Tegucigalpa, Honduras, in 1977. He received the B.S. degree in electrical and computer engineering at the Georgia Institute of Technology, Atlanta, in 1999. He is currently working there as graduate research assistant and pursuing the M.S. and Ph.D. degrees in electrical and computer engineering.

His research interests are mainly in fabrication technology and applications for wireless ceramic pressure sensors.

Jennifer M. English received the B.S., M.S., and Ph.D. degrees in electrical engineering from the Georgia Institute of Technology, Atlanta, in 1993, 1996, and 2000, respectively.

Currently, she is an Assistant Professor in the Department of Electrical and Computer Engineering at the University of Alabama, Huntsville. She is also a member of the LICOS research center. Her research interests include ceramic-based MEMS actuators and integrated MEMS/photonic devices and systems.

Martin von Arx received the diploma in physics from the Swiss Federal Institute of Technology, ETH Zurich, Switzerland, in 1993. He then studied thermoelectrical properties of standard IC MEMS materials at the Physical Electronics Laboratory, ETH Zurich. After receiving the Ph.D. degree in 1998, he did postgraduate studies in the microsensors and microactuators group, Georgia Institute of Technology, Atlanta.

Currently, he is head of the key function "ultrasonics and force" in the BU wirebonder at ESEC SA (Cham, Switzerland) and developing a new ultrasonic transducer.

Mark G. Allen (M'89) received the B.A. degree in chemistry, the B.S.E. degree in chemical engineering, and the B.S.E. degree in electrical engineering, all from the University of Pennsylvania, Philadelphia, and M.S. and Ph.D. degrees from the Massachusetts Institute of Technology (MIT), Cambridge.

Since 1989, he has been at the Georgia Institute of Technology, Atlanta, where he currently holds the rank of Professor. His research interests include micromachining fabrication technology, magnetic micromachined devices, and materials issues in micromachined structures and electronic packaging.

Dr. Allen was General Co-Chairman of the 1996 IEEE/ASME Microelectromechanical Systems Conference and is a Member of the Editorial Board of the *Journal of Microelectromechanics and Microengineering.*